

Toward Unified Multimodal Representation Learning for Autonomous Driving

Ximeng Tao¹, Dimitar Filev¹, Gaurav Pandey²

Abstract—Contrastive Language-Image Pre-training (CLIP) has shown impressive performance in aligning visual and textual representations. Recent studies have extended this paradigm to 3D vision to improve scene understanding for autonomous driving. A common strategy is to employ pairwise cosine similarity between modalities to guide the training of a 3D encoder. However, considering the similarity between individual modality pairs rather than all modalities jointly fails to ensure consistent and unified alignment across the entire multimodal space. In this paper, we propose a Contrastive Tensor Pre-training (CTP) framework that simultaneously aligns multiple modalities in a unified embedding space to enhance end-to-end autonomous driving. Compared with pairwise cosine similarity alignment, our method extends the 2D similarity matrix into a multimodal similarity tensor. Furthermore, we introduce a tensor loss to enable joint contrastive learning across all modalities. For experimental validation of our framework, we construct a text–image–point cloud triplet dataset derived from existing autonomous driving datasets. The results show that our proposed unified multimodal alignment framework achieves favorable performance for both scenarios: (i) aligning a 3D encoder with pretrained CLIP encoders, and (ii) pretraining all encoders from scratch. Codes are available at: <https://github.com/TAMU-CVRL/CTP>.

I. INTRODUCTION

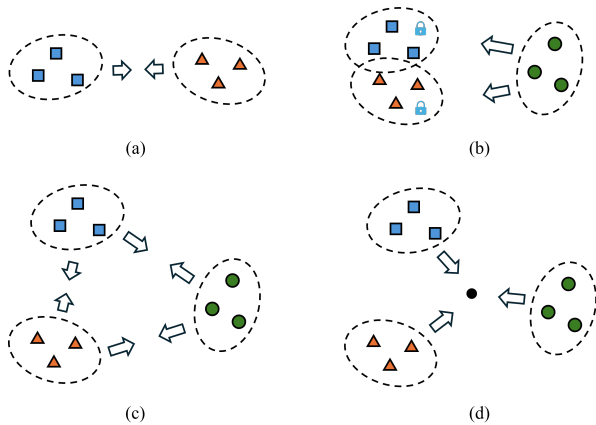


Fig. 1. Overview of different contrastive representation learning methods. (a) CLIP: aligns two modalities. (b) Aligns a third modality with two already aligned modalities. (c) Performs pairwise alignment between every modality pair. (d) CTP: aligns all modalities toward one point.

Large Language Models (LLMs) have demonstrated remarkable performance in the textual modality, as well as

¹Ximeng Tao and Dimitar Filev are with J. Mike Walker '66 Department of Mechanical Engineering, Texas A&M University, College Station, TX 77843, USA [ximeng](mailto:ximeng@tamu.edu), dfilev@tamu.edu

²Gaurav Pandey is with The Department of Engineering Technology and Industrial Distribution Texas A&M University, College Station, TX 77843, USA gpandey@tamu.edu

strong capabilities in scene understanding, reasoning, and decision-making [1]. Furthermore, Vision–Language Models (VLMs) have achieved the ability to jointly understand visual and textual domains [2], [3], [4], which significantly benefits End-to-End (E2E) autonomous driving [5], [6], [7], [8], [9], [10]. Recently, there has been growing interest in extending the capabilities of LLMs from 2D to 3D domains [11], [12], [13], [14]. Point clouds are a common representation of 3D information. They provide accurate spatial understanding and are robust to variations in illumination and adverse weather conditions, making 3D perception a critical capability for autonomous driving. However, LiDAR point clouds suffer from issues such as data sparsity, model scalability, and computational inefficiency [15], which limit effective 3D representation alignment.

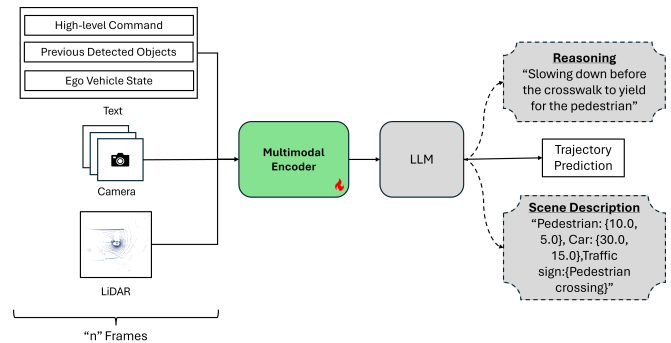


Fig. 2. Overview of the multimodal language model–based end-to-end autonomous driving system. The multimodal encoder is pretrained to align all modalities within a unified embedding space, enabling the LLM to jointly understand cross-modal information and generate reasoning, scene descriptions, and future trajectory predictions. In this work, we primarily focus on training the “Multimodal Encoder” that can be used in an end-to-end driving system as shown here.

CLIP [16] provides an effective approach for aligning textual and visual modalities (Fig. 1a). The pretrained Vision Transformer (ViT) [17] can serve as the image encoder, forming the vision tower for LLMs [2]. Inspired by the CLIP framework, several studies have explored extending the CLIP embedding space to point clouds [18], [19], showing improved scene understanding [20], [21], [22], localization [23], semantic segmentation [24], and object detection [25], [26]. A common strategy is to use contrastive learning to align 3D representations with CLIP text embeddings [18] or image embeddings [27], or to align them with both modalities through a similarity matrix [28], [29], [30], [31] (Fig. 1b, c). However, these alignment operations remain limited to pairwise cosine similarity between modalities, rather than

jointly aligning all modalities in a unified framework [32].

Our goal is to design a framework that simultaneously aligns multiple modalities (Fig. 1d). The resulting aligned multimodal encoder can then be integrated into an end-to-end autonomous driving system to jointly understand heterogeneous inputs, including images, text, Radar, and LiDAR, as illustrated in Fig. 2. In this paper, we propose a simple yet effective Contrastive Tensor Pre-training (CTP) framework that unifies the alignment of multiple modalities. Specifically, we focus on three modalities in this work: text, image, and point cloud. Unlike text–image pairs, which have large-scale data readily available on the Internet, there is a lack of text–image–point cloud datasets, making it difficult to perform a triple-modality alignment. First, we introduce a method to construct a triplet training dataset based on the existing autonomous driving dataset nuScenes [33]. Using the same procedure, we also build three triplet datasets derived from nuScenes [33], KITTI [34], and the Waymo Open Perception Dataset (WOD-P) [35] for testing. Second, we propose a similarity tensor that captures all possible combinations among multiple modalities. We further analyze the differences between cosine similarity and L2-norm similarity in high-dimensional multimodal alignment. Third, as the number of modalities increases, the cross-entropy loss originally computed along a row or column is extended to a tensor-based loss. To efficiently compute this loss, we propose three different flattening strategies to reduce the high-dimensional tensor into a one-dimensional vector, enabling straightforward cross-entropy computation.

To evaluate the feasibility and effectiveness of our framework, we conduct zero-shot classification experiments on the constructed triplet datasets. We conduct experiments under two training settings: (i) training only the point cloud encoder while keeping the CLIP text and image encoders frozen, and (ii) pretraining all encoders. Our method is primarily compared with pairwise cosine similarity matrix–based approaches [28], [30]. When training only the point cloud encoder, CTP surpasses the pairwise cosine similarity method by +5.42%, +8.13%, and +1.21% on the nuScenes, KITTI, and WOD-P datasets, respectively. With all encoders pretrained, the improvements increase to +13.91%, +40.87%, and +11.50%.

II. RELATED WORK

A. Multimodal Alignment

Multimodal alignment has gained increasing attention for its ability to enable models to handle diverse multimodal tasks. Vision–language pre-training [36], [37] has recently achieved remarkable success across various downstream applications. Pioneering works such as CLIP [16] and ALIGN [38] focus on visual and textual modalities, demonstrating effective alignment between the two representations. Various methods have adapted CLIP to extract video [39], audio [40], and 3D representations [41]. Beyond alignment between two modalities, ImageBind [42] introduced a multimodal pre-training framework that leverages the image modality as a bridge to bind all modalities together.

LanguageBind [43] instead employs the text modality as the alignment anchor to further enhance multimodal representation learning. However, most existing methods rely on pairwise cosine similarity between two modalities rather than jointly aligning all modalities. A unified framework for pre-training across multiple modalities remains underexplored, limiting the potential of multimodal representation learning. To address this limitation, we extend the CLIP framework from a 2D similarity matrix to an n -dimensional similarity tensor.

B. 3D Representation Learning

Recently, there has been growing interest in connecting 3D point clouds with natural language through vision–language pre-training frameworks. Early works such as PointCLIP [18], PointCLIP v2 [41], and CLIP2Point [44] explore transferring CLIP’s image–text alignment capability to 3D understanding. While these approaches perform well on dense object point clouds, they are less effective for sparse automotive objects with heavy occlusions. Lidar-CLIP [27] adapts CLIP to the LiDAR domain by aligning LiDAR features with pretrained CLIP image encoders, but it still relies solely on pairwise cosine similarity between the two modalities. Subsequent methods, including CLIP² [28], TriCLIP-3D [45], Uni3D [46] and OpenShape [47], extend multimodal contrastive learning to broader 3D representation tasks. ULIP [30], [48] and CLIP goes 3D [29] further integrate pretrained 2D vision–language models with point cloud encoders, highlighting the potential of unified 3D–language pre-training for downstream recognition and retrieval. Different from these approaches, our proposed CTP framework jointly aligns point cloud, image, and text encoders into a unified representation space, achieving stronger and more consistent performance in E2E autonomous driving.

III. METHODOLOGY

A. Triplet Dataset

Due to the lack of large-scale text–image–point cloud triplet datasets, we construct our own triplet dataset for pretraining and evaluation. In this work, we particularly focus on outdoor scenarios and utilize sparse and challenging LiDAR point clouds from existing autonomous driving datasets. Typically, an autonomous driving dataset \mathcal{D} consists of multiple scenes, each containing a sequence of frames. For each frame indexed by t , we obtain the corresponding camera images X_I^t , the LiDAR point cloud X_P^t , and the set of annotated 3D bounding boxes $X_B^t = \{B_t^k\}_{k=1}^{K_t}$, where K_t denotes the number of detected objects in frame t .

We define an extraction algorithm $\Phi(\cdot)$ that, for each bounding box B_t^k , extracts the corresponding point cloud segment P_t^k , cropped image region I_t^k , and textual annotation $(T_A)_t^k$. Formally,

$$((T_A)_t^k, I_t^k, P_t^k) = \Phi(X_I^t, X_P^t, B_t^k), \quad (1)$$

where t indexes frames and k indexes objects within each frame. This yields an initial triplet dataset

$$\mathcal{D}_{\text{tri}} = \{((T_A)_t^k, I_t^k, P_t^k)\}_{t,k}. \quad (2)$$

Since the original annotations $(T_A)_t^k$ are often short and lack descriptive detail, VLM [49], [2], [50] is employed to generate richer pseudo captions $(T_G)_t^k$, conditioned on the annotation, the cropped image, and a textual prompt \mathcal{Q} defined as: "Provide one factual sentence describing its visual attributes..."

$$(T_G)_t^k = \text{VLM}((T_A)_t^k, I_t^k, \mathcal{Q}). \quad (3)$$

This process converts the initial triplet dataset \mathcal{D}_{tri} into a collection of semantically aligned text-image-point cloud triplets,

$$\overline{\mathcal{D}}_{\text{tri}} = \{((T_G)_t^k, I_t^k, P_t^k)\}_{t,k}, \quad (4)$$

which serves as the foundation for unified multimodal pre-training and evaluation.

B. Similarity Tensor

The alignment between two modalities can be effectively achieved through contrastive training using a cosine similarity matrix [16]. Naturally, when extending to more than two modalities, a common approach is to perform pairwise contrastive training between each pair of modalities using separate cosine similarity matrices [30], [28], [29]. However, such pairwise similarity losses do not capture global relationships across all modalities simultaneously. Consider a scenario with q modalities and a mini-batch size of b . Within a single mini-batch, the total number of possible similarity combinations is b^q . However, when using pairwise similarity matrices, each matrix captures only b^2 pairwise relationships, and the total number of considered relationships becomes $\frac{q(q-1)}{2} \times b^2$. As q increases, this number becomes significantly smaller than the true number of similarity combinations b^q , thereby limiting the model's ability to learn global alignment across all modalities. To address this limitation and achieve joint alignment across all modalities, we extend the similarity matrix into a similarity tensor. Due to the lack of large-scale multimodal datasets and to simplify experimentation while verifying the feasibility of our framework, we focus on three modalities in this work: text, LiDAR point cloud, and image, denoted as T , P , and I , respectively. In this case, the similarity tensor can be viewed as a cube of size b^3 .

We first establish the matrix-based contrastive loss \mathcal{L}_{2D} as a baseline for comparison. Extending CLIP [16] to three modalities, the overall pairwise contrastive loss can be formulated as [30]:

$$\mathcal{L}_{2D} = \alpha_1 \cdot \mathcal{L}_{T-I} + \beta_1 \cdot \mathcal{L}_{T-P} + \gamma_1 \cdot \mathcal{L}_{P-I}, \quad (5)$$

where \mathcal{L}_{T-I} , \mathcal{L}_{T-P} , and \mathcal{L}_{P-I} represent the contrastive losses between the text-image, text-point, and point-image modality pairs, respectively. The coefficients α_1 , β_1 , and γ_1 are weighting factors. However, aligning all three modalities by summing pairwise similarity matrices covers only $3 \times b^2$ pairs, which is substantially fewer than the total b^3 possible similarity combinations. This leads to an incomplete comparison problem. To achieve full multimodal alignment, we

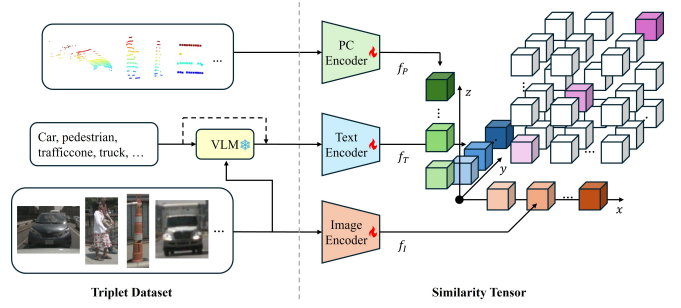


Fig. 3. **Overview of CTP framework.** Triplet dataset: LiDAR point clouds, cropped images, and annotations are extracted from autonomous driving datasets to form triplet samples. The annotation expanded into a detailed caption using a VLM. similarity tensor: Image, text, and point cloud features are arranged along the x , y , and z axes to form a 3D similarity tensor. Each element represents a unique combination of three features, and the similarity measures their relationships. During training, the similarity scores of the matched triplets (small purple cubes) are maximized using a cross-entropy loss.

propose extending the similarity matrix into a similarity tensor, which generalizes contrastive learning beyond pairwise modality relationships.

As shown in Fig. 3, triplets are fed into the text encoder E_{text} , image encoder E_{img} , and point cloud encoder E_{pc} , which output text features $f_T \in \mathbb{R}^d$, image features $f_I \in \mathbb{R}^d$, and point cloud features $f_P \in \mathbb{R}^d$, respectively, where d denotes the embedding dimension. These features are then normalized as \hat{f}_T , \hat{f}_I , and \hat{f}_P using $\hat{f} = f/|f|$, and together they form a similarity tensor. In a cosine similarity matrix, the similarity between two modality vectors is measured by their dot product, e.g., $\hat{f}_T \cdot \hat{f}_I$. A natural question arises: *how can we compute the similarity among multiple normalized vectors?*

We denote $\mathcal{S}^{(i,j,k)}$ as the similarity score of each element in the similarity tensor, computed from \hat{f}_T , \hat{f}_I , and \hat{f}_P , where i , j , and k represent the indices corresponding to text, image, and point cloud features, respectively. A common approach is to compute pairwise cosine similarities and aggregate them to obtain an overall multi-modal similarity score. Since normalized feature vectors lie on a hypersphere, Euclidean distance can also serve as a valid similarity measure. Notably, we use the L2-norm without squaring it. Otherwise, the resulting metric becomes linearly dependent on cosine similarity, making the two measures equivalent.

The cosine tensor similarity $\mathcal{S}_{\text{cos}}^{(i,j,k)}$ is defined as follows:

$$\mathcal{S}_{\text{cos}}^{(i,j,k)} = \frac{1}{3} \left(\hat{f}_I^i \cdot \hat{f}_T^j + \hat{f}_I^i \cdot \hat{f}_P^k + \hat{f}_T^j \cdot \hat{f}_P^k \right), \quad (6)$$

and the L2-norm tensor similarity $\mathcal{S}_{L_2}^{(i,j,k)}$ is:

$$\mathcal{S}_{L_2}^{(i,j,k)} = \|\hat{f}_I^i - \hat{f}_T^j\|_2 + \|\hat{f}_I^i - \hat{f}_P^k\|_2 + \|\hat{f}_T^j - \hat{f}_P^k\|_2. \quad (7)$$

The L2-norm tensor similarity $\mathcal{S}_{L_2}^{(i,j,k)}$ is subsequently scaled in Eq. 8. Both similarity functions can be generalized to more modalities by introducing additional pairwise terms. To ensure that the similarity score approaches 1 when all feature vectors are close to each other, we apply a simple

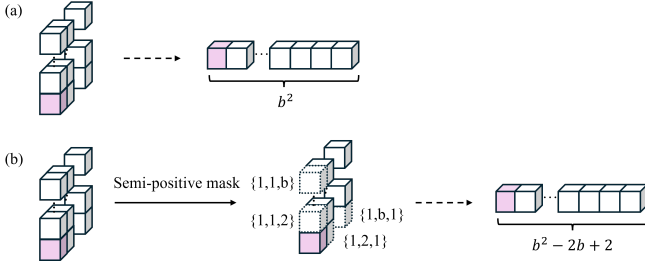


Fig. 4. Different strategies for flattening the plane loss: (a) **nm**: direct flattening without masking, (b) **mask**: masking duplicated entries, CTP adopts (b) as the standard flattening strategy.

mapping from \mathcal{S}_{L_2} to $\tilde{\mathcal{S}}_{L_2}$ using Eq. 8.

$$\tilde{\mathcal{S}}_{L_2} = 1 - \frac{\mathcal{S}_{L_2}}{L_{\max}}, \quad (8)$$

where L_{\max} denotes the maximum possible Euclidean distance between points on a unit hypersphere [51]. For $q = 3$, $L_{\max} = 3\sqrt{3}$. In this paper, we primarily employ $\tilde{\mathcal{S}}_{L_2}$ to measure the similarity among the three modalities.

C. Tensor Loss

In the similarity matrix, the contrastive loss is computed based on the target’s corresponding row and column, which form a one-dimensional structure [16]. Within this 1D space, the objective is to increase the target similarity while reducing the similarity of all other elements during training. Analogously, in the similarity tensor, we extend this concept by generalizing the 1D loss into a 2D tensor loss, referred to as the plane loss. Instead of optimizing similarities along a single row or column, contrastive learning is performed across an entire plane within the similarity tensor. For the similarity tensor, the loss along one axis is computed as follows. Given a batch size of b , there are b such planes. Each plane is flattened into a one-dimensional vector, where the ground-truth similarity is assigned to the corresponding target position. The loss is then computed using this vector representation.

We propose two different strategies for flattening a plane into a single line, as illustrated in Fig. 4. The simplest approach is to directly flatten all elements into a row of length b^2 . However, we observe that when the similarity matrix is extended to a similarity tensor, some of the terms in the similarity tensor have duplicated features, for example, in a case like $\{1, 1, 2\}$ (Fig. 4b), the first and second features are same, we propose to mask those elements and flatten the remaining values into a row of length $b^2 - 2b + 2 (< b^2)$. This masking strategy not only decreases the computational complexity of training but also improves the overall performance of the model because the duplicated entries of the similarity tensor adversely affects the optimization.

We denote the two flattening strategies described above as $\text{FLAT}(\cdot)$. Since the similarity tensor contains b planes, the flattening operation yields b vectors, which are stacked to form a matrix. We then apply the cross-entropy (CE) loss over this matrix to compute the plane loss, formulated as:

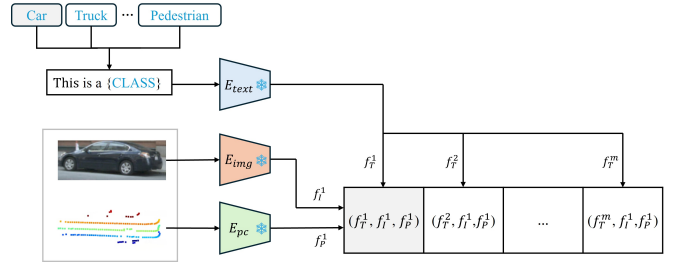


Fig. 5. Zero-shot classification. Each image–point cloud pair is compared with all text features, and the class is determined by the highest L2-norm similarity. When computing similarity between point cloud or image features and text features only, cosine similarity is employed.

$$\mathcal{L}_{uv} = \sum_{\ell=1}^b \text{CE} \left(\text{FLAT} \left(\tilde{\mathcal{S}}_{L_2}^{(i,j,k)} \right) \right), \quad (9)$$

where $uv \in \{ij, ik, jk\}$ denotes the selected plane, and the index $\ell = i, j, k$ corresponds to the axis orthogonal to that plane. In this work, the total loss of our CTP framework is computed as the sum of the three plane losses:

$$\mathcal{L}_{3D} = \alpha_2 \mathcal{L}_{jk} + \beta_2 \mathcal{L}_{ik} + \gamma_2 \mathcal{L}_{ij}. \quad (10)$$

The coefficients α_2 , β_2 , and γ_2 are weighting factors. For complete comparison, they are all set to $\frac{1}{3}$.

D. Zero-Shot Classification

Once the three encoders E_{img} , E_{pc} and E_{text} are trained using the loss function described in equation (10) and the triplet training dataset described in section III-A, we use zero-shot classification to validate the encoder performance. Zero-shot classification aims to assign class labels to unseen samples without task-specific fine-tuning. A common approach is to compute feature representations for all class texts and then assign each LiDAR point cloud feature to the nearest class based on its similarity score. As shown in Fig. 5, this concept easily extends to three modalities, using image–point cloud pairs as input, while the image input remains optional. Let m class texts be formulated as prompts and encoded by the pretrained text encoder E_{text} . The image–point cloud pairs are processed by their respective pretrained encoders, E_{img} and E_{pc} , to obtain normalized features \hat{f}_T , \hat{f}_I , and \hat{f}_P . The L2-norm similarity score $\tilde{\mathcal{S}}_{L_2}$ is then computed between the m text features \hat{f}_T and the image–point cloud features (\hat{f}_I, \hat{f}_P) , and the class with the highest similarity score is assigned to each pair.

IV. EXPERIMENTS

A. Datasets

a) *Training Datasets*: We use the nuScenes dataset [33] to construct a triplet training dataset. The nuScenes `trainval` split contains 850 scenes with 23 object classes and accurately annotated 3D bounding boxes. We use the `train` split to generate our training dataset. For each frame, we extract the point cloud segment within each bounding box, the corresponding cropped image region, and the associated

TABLE I
ZERO-SHOT CLASSIFICATION ACCURACY (%) ON THE NUSCENES TRIPLET DATASET

Data	Method	Avg.	Car	Truck	Bus	Ped.	Bicycle	Trailer	C.V.	Motor.	Barrier	T.C.
Depth	pointCLIP [18]	17.29	0.14	0.00	0.00	0.27	0.13	5.01	0.00	0.00	98.72	0.00
	pointCLIP V2 [41]	5.41	0.08	0.00	0.05	2.78	0.63	0.00	77.29	0.58	21.52	0.00
	CLIP2Point [44]	16.63	0.00	0.18	0.00	8.21	1.89	0.00	1.49	0.81	87.84	0.12
I-P	LidarCLIP* [27]	73.35	74.69	43.58	84.61	84.14	78.24	59.05	9.46	73.58	76.02	97.73
T_G -I-P	CLIP ^{2*} [28]	74.66	70.66	44.13	66.99	86.65	59.12	77.47	2.19	63.27	94.09	96.45
	CTP (Ours)	80.08	77.84	69.92	60.98	94.79	64.29	60.00	0.00	46.43	91.83	95.24

textual annotation T_A as defined in Eq. 1. During dataset construction, we filter out point clouds containing fewer than 5 points and discard images in which an object is less than 40% visible. To enrich the textual descriptions, we employ Qwen3-VL-8B-Instruct [49] to generate detailed pseudo-captions T_G , resulting in an augmented dataset as formulated in Eq. 3. This enhanced version is used as the standard training dataset. The final dataset contains approximately $\sim 322K$ triplets.

b) Test Datasets: The same preprocessing procedure is applied to the nuScenes validation split to construct a nuScenes triplet validation dataset containing $\sim 68K$ triplets. To test the generalization of zero-shot classification on other datasets, we additionally use KITTI [34] and the WOD-P [35]. For KITTI, we construct a triplet dataset following the same procedure described above, while filtering out point clouds with fewer than 15 points. This results in $\sim 24K$ triplets. For WOD-P, we apply the same preprocessing as for KITTI. Since the WOD-P is extremely large, we use only the first 50 segments of the validation split for the test. Each segment contains 20 frames, from which we sample 5 frames at 4-second intervals, yielding $\sim 34K$ triplets in total.

B. Implementation Details

a) Encoders: We use the CLIP ViT-B/32 text and image encoders, where the text encoder is a Transformer-based language model [52] and the image encoder is a ViT [17]. Each cropped image is letterbox-resized to 224×224 and normalized using the CLIP mean and standard deviation. For point cloud processing, we adopt the lightweight PointNet++ [53]. Since the input layer requires a fixed number of 1024 points, each point cloud is preprocessed accordingly. Point clouds containing fewer than 1024 points are zero-padded, while those with more than 1024 points are downsampled to 1024 using the farthest point sampling (FPS) algorithm [53]. In addition, a linear projection layer is applied to map the PointNet++ output features into a 512-dimensional embedding space, ensuring consistency with the CLIP text and image representations.

b) Pre-training: (i) When freezing the CLIP text and image encoders and pretraining only the point cloud encoder, we employ the AdamW optimizer [54] with a weight decay of 0.2 [55] and an initial learning rate of 5×10^{-4} . A warm-up ratio of 0.1 is used, followed by a constant learning rate schedule. The learnable temperature parameter is initialized

TABLE II
ZERO-SHOT CLASSIFICATION ACCURACY (%) ON THE KITTI AND WOD-P TRIPLET DATASETS

Method	KITTI	Waymo
pointCLIP [18]	9.63	13.79
pointCLIP V2 [41]	9.44	14.31
CLIP2Point [44]	10.35	21.27
LidarCLIP* [27]	67.79	75.27
CLIP ^{2*} [28]	74.55	84.86
CTP (Ours)	82.68	86.07

to 0.07. Training is conducted for 20 epochs with a batch size of 192 on a single RTX 4090 GPU. (ii) When pretraining all encoders, we use the AdamW optimizer with the same hyperparameters as above. Training is performed for 10 epochs with a total batch size of 384, and all models are trained on two A100 40G GPUs. In (i) and (ii), all models use the final checkpoint for zero-shot classification.

C. Zero-shot Classification

We adopt a zero-shot classification setup as described previously in Fig. 5. For each dataset, we define a set of text templates and generate prompts in the format "This is a {CLASS}", with CLASS denoting the object annotation. We then apply the three trained encoders to extract the corresponding features. The image feature is optional, but we observe that incorporating both image and point cloud inputs improves classification accuracy. Therefore, all models are evaluated using joint point cloud-image inputs whenever applicable.

a) Point Cloud Encoder: In Table I and II, the image and text encoders are frozen, and only the point cloud encoder is trained. The * symbol indicates that the corresponding method is retrained on our nuScenes triplet dataset. Although the proposed CTP framework is designed for pre-training multiple encoders jointly, most previous works focus on training a point cloud encoder using pretrained CLIP image and text encoders. To ensure a fair comparison, we follow their training strategy and retrain their models on our nuScenes triplet training set, and use the point cloud encoder, pointnet++ [53]. Table I shows the zero-shot classification performance of different methods. PointCLIP [18], PointCLIP v2 [41], and CLIP2Point [44] achieve strong performance on dense, single-object point clouds by converting them into depth images. In this work,

TABLE III
ZERO-SHOT CLASSIFICATION ACCURACY (%) ON THE NUSCENES TRIPLET DATASET

Method	Avg.	Car	Truck	Bus	Ped.	Bicycle	Trailer	C.V.	Motor.	Barrier	T.C.
ULIP* [30]	52.01	37.79	43.49	64.05	79.48	45.41	33.89	43.92	68.37	67.80	42.76
CTP-nm	62.23	50.99	14.29	56.10	95.26	78.57	56.67	23.53	78.57	86.06	79.37
CTP	65.92	62.16	4.51	78.05	91.94	71.43	60.00	47.06	96.43	88.46	52.38

TABLE IV
ZERO-SHOT CLASSIFICATION ACCURACY (%) ON THE KITTI AND WOD-P TRIPLET DATASETS

Method	KITTI					Waymo			
	Avg.	Car	Truck	Van	Ped.	Avg.	Car	Sign	Ped.
ULIP* [30]	44.05	38.26	46.10	39.60	95.82	53.18	43.62	87.40	68.92
CTP-nm	75.42	81.56	25.00	31.25	92.86	63.18	61.54	92.86	43.33
CTP	84.92	92.20	25.00	37.50	100.00	64.68	63.64	89.29	46.67

TABLE V
COMPARISON OF DIFFERENT METHODS FOR MEASURING SIMILARITY

Method	Dataset	Average Accuracy (%)		
		T-I	T-P	T-(I, P)
ULIP* [30]	nuScenes	49.55	37.65	52.01
CTP w/ Cosine similarity		47.43	38.27	48.85
CTP w/ L2-norm similarity		61.34	57.34	65.92
ULIP* [30]	KITTI	53.16	17.91	44.05
CTP w/ Cosine similarity		69.61	52.9	70.95
CTP w/ L2-norm similarity		78.09	82.57	84.92
ULIP* [30]	Waymo	52.45	42.38	53.18
CTP w/ Cosine similarity		72.24	45.07	69.15
CTP w/ L2-norm similarity		59.92	70.98	64.68

we first normalize LiDAR-based point cloud objects and directly evaluate these models. However, real-world LiDAR point clouds are inherently sparse and noisy, with each object often exhibiting incompleteness, self-occlusion, and irregular sampling density, which leads to suboptimal performance. LidarCLIP [27] is designed for scene-level representation learning by transferring the pretrained CLIP image encoder to a point cloud encoder. In this work, we follow the same idea and retrain the model with a focus on object-level representation. Without the assistance of textual features, its average classification accuracy is 73.35% lower than that of methods utilizing all three modalities. CLIP² [28] aligns a point cloud encoder with pretrained CLIP text and image encoders using two cosine similarity matrices, as described in Eq. 5, where $\alpha_1 = 0$ and $\beta_1 = \gamma_1 = \frac{1}{2}$. The dataset uses T_G , which provides more descriptive pseudo captions generated by a VLM. For example, the short annotation "A car" becomes "A white van with a boxy geometry and visible rear windows is parked." Results demonstrate that the similarity tensor provides richer cross-modal information, leading to improved alignment. We observe that the *Trailer* and *Motorcycle* (Motor) classes still require more high-quality samples to further improve performance. The *Construction Vehicle* (C.V.) class contains relatively few samples, causing

most methods to misclassify it as *Truck*. Overall, CTP achieves an accuracy of 80.08%, surpassing all other methods. We further compare the results on the unseen datasets, KITTI and WOD-P. As shown in Table II, our method CTP outperforms other methods and achieves +8.13% and +1.21% improvement compared to the cosine similarity matrix-based method CLIP².

b) All Encoders: In Table III, IV, and V, all three encoders (image, text, and point cloud) are jointly trained. CTP-nm indicates the no masking strategies described in Fig. 4. The primary goal of our method is to perform contrastive pre-training across all encoders simultaneously. Due to dataset limitations, we verify our framework using three modalities. To evaluate our approach, we compare it with pairwise cosine similarity matrix-based methods by pre-training all encoders jointly and conducting the experiments. We select ULIP [30] as the representative pairwise cosine similarity matrix-based method. In that work, Eq. 5 is used with $\alpha_1 = 0$ to train only the point cloud encoder, and we use the same setting when training CLIP² in the previous paragraph. In this paragraph, we set all coefficients to $\alpha_1 = \beta_1 = \gamma_1 = \frac{1}{3}$ to train all encoders.

As shown in Table III, we compare ULIP with two variants of our proposed CTP framework (with and without masking). Both CTP variants outperform ULIP, which achieves 52.01% accuracy, with CTP reaching the highest accuracy of 65.92%. Compared to Table I, where only the point cloud encoder is trained, the overall performance here is lower. This decrease is mainly attributed to the smaller dataset size and reduced data richness. The strong geometric similarity between *Truck* and *Bus* in the dataset further leads to lower accuracy in *Truck* class. Nevertheless, Table III demonstrates the feasibility of our framework and its ability to effectively align multiple modalities, surpassing pairwise cosine similarity matrix-based approaches.

Similarly, we conduct experiments on the KITTI and WOD-P triplet datasets, as shown in Table IV. The KITTI dataset originally contains nine categories. During experiments, we merge the *Person sitting* and *Cyclist* categories into the *Pedestrian* class, resulting in four classes while

ignoring the remaining categories. For WOD-P, which contains four categories, we merge the *Cyclist* category into *Pedestrian*, leaving three classes for testing. The results again demonstrate that all three CTP variants significantly outperform ULIP on both datasets. The standard CTP achieves the best performance, surpassing ULIP by +40.87% and +11.50% on KITTI and WOD-P, respectively. We observe that all methods achieve high accuracy on the *Pedestrian* class, which can be attributed to the small size of the KITTI triplet dataset, which contains only 1590 *pedestrian* samples. We attribute this improvement to the fact that, unlike pairwise modality alignment, our method jointly aligns all modalities toward a single point, enabling more efficient alignment within the same number of training epochs. Notably, in Table III and Table V, CTP outperforms CTP-nm highlighting the need for properly masking duplicated elements.

D. Analyses

In Table V, we compare the representation alignment among three modalities after pre-training. We train our proposed CTP method using both the L2-norm similarity and cosine similarity to compute similarity scores \tilde{S}_{L2} and S_{\cos} , and conduct experiments on three triplet datasets. First, we observe that the standard CTP model consistently achieves the best performance across all datasets, regardless of whether single-modality or bimodal inputs are used. Moreover, when comparing classification accuracy under different input configurations, joint multimodal inputs generally outperform single-modality inputs. In addition, comparing CTP variants using cosine similarity and L2-norm similarity shows that L2-norm similarity provides better multimodal alignment in our framework, resulting in improved representation learning across the three modalities.

V. CONCLUSIONS

We propose CTP, a contrastive pre-training framework that aligns multiple modalities via a similarity tensor. In contrast to previous pairwise cosine similarity matrix-based methods, our approach uses an n -dimensional similarity tensor, enabling comprehensive alignment across all modalities. We further evaluate the impact of different similarity measures, including cosine similarity and L2-norm similarity. Experimental results demonstrate the feasibility and efficiency of CTP in three-modality representation learning, highlighting its potential to align multi-sensor modalities and enhance applications such as E2E driving systems through improved multi-sensor understanding.

REFERENCES

- [1] T. Brown, B. Mann, N. Ryder, M. Subbiah, J. D. Kaplan, P. Dhariwal, A. Neelakantan, P. Shyam, G. Sastry, A. Askell, *et al.*, "Language models are few-shot learners," *Advances in neural information processing systems*, vol. 33, pp. 1877–1901, 2020.
- [2] H. Liu, C. Li, Q. Wu, and Y. J. Lee, "Visual instruction tuning," *Advances in neural information processing systems*, vol. 36, pp. 34 892–34 916, 2023.
- [3] J. Li, D. Li, S. Savarese, and S. Hoi, "Blip-2: Bootstrapping language-image pre-training with frozen image encoders and large language models," in *International conference on machine learning*. PMLR, 2023, pp. 19 730–19 742.
- [4] J.-B. Alayrac, J. Donahue, P. Luc, A. Miech, I. Barr, Y. Hasson, K. Lenc, A. Mensch, K. Millican, M. Reynolds, *et al.*, "Flamingo: a visual language model for few-shot learning," *Advances in neural information processing systems*, vol. 35, pp. 23 716–23 736, 2022.
- [5] L. Chen, O. Sinavski, J. Hünemann, A. Karnsund, A. J. Willmott, D. Birch, D. Maund, and J. Shotton, "Driving with llms: Fusing object-level vector modality for explainable autonomous driving," in *2024 IEEE International Conference on Robotics and Automation (ICRA)*. IEEE, 2024, pp. 14 093–14 100.
- [6] J.-J. Hwang, R. Xu, H. Lin, W.-C. Hung, J. Ji, K. Choi, D. Huang, T. He, P. Covington, B. Sapp, *et al.*, "Emma: End-to-end multimodal model for autonomous driving," *arXiv preprint arXiv:2410.23262*, 2024.
- [7] Y. Ma, T. Wei, N. Zhong, J. Mei, T. Hu, L. Wen, X. Yang, B. Shi, and Y. Liu, "Leapvad: A leap in autonomous driving via cognitive perception and dual-process thinking," *arXiv preprint arXiv:2501.08168*, 2025.
- [8] S. Xing, C. Qian, Y. Wang, H. Hua, K. Tian, Y. Zhou, and Z. Tu, "Openemma: Open-source multimodal model for end-to-end autonomous driving," in *Proceedings of the Winter Conference on Applications of Computer Vision*, 2025, pp. 1001–1009.
- [9] X. Zhou, X. Han, F. Yang, Y. Ma, and A. C. Knoll, "Opendrivelva: Towards end-to-end autonomous driving with large vision language action model," *arXiv preprint arXiv:2503.23463*, 2025.
- [10] X. Huang, E. M. Wolff, P. Vernaza, T. Phan-Minh, H. Chen, D. S. Hayden, M. Edmonds, B. Pierce, X. Chen, P. E. Jacob, *et al.*, "Drivegpt: Scaling autoregressive behavior models for driving," *arXiv preprint arXiv:2412.14415*, 2024.
- [11] Y. Hong, H. Zhen, P. Chen, S. Zheng, Y. Du, Z. Chen, and C. Gan, "3d-llm: Injecting the 3d world into large language models," *Advances in Neural Information Processing Systems*, vol. 36, pp. 20 482–20 494, 2023.
- [12] S. Yang, J. Liu, R. Zhang, M. Pan, Z. Guo, X. Li, Z. Chen, P. Gao, H. Li, Y. Guo, *et al.*, "Lidar-llm: Exploring the potential of large language models for 3d lidar understanding," in *Proceedings of the AAAI Conference on Artificial Intelligence*, vol. 39, no. 9, 2025, pp. 9247–9255.
- [13] B. Chen, Z. Xu, S. Kirmani, B. Ichter, D. Sadigh, L. Guibas, and F. Xia, "Spatialvlm: Endowing vision-language models with spatial reasoning capabilities," in *Proceedings of the IEEE/CVF Conference on Computer Vision and Pattern Recognition*, 2024, pp. 14 455–14 465.
- [14] J. Kerr, C. M. Kim, K. Goldberg, A. Kanazawa, and M. Tancik, "Lerf: Language embedded radiance fields," in *Proceedings of the IEEE/CVF international conference on computer vision*, 2023, pp. 19 729–19 739.
- [15] X. Ma, Y. Bhalgat, B. Smart, S. Chen, X. Li, J. Ding, J. Gu, D. Z. Chen, S. Peng, J.-W. Bian, *et al.*, "When llms step into the 3d world: A survey and meta-analysis of 3d tasks via multi-modal large language models," *arXiv preprint arXiv:2405.10255*, 2024.
- [16] A. Radford, J. W. Kim, C. Hallacy, A. Ramesh, G. Goh, S. Agarwal, G. Sastry, A. Askell, P. Mishkin, J. Clark, *et al.*, "Learning transferable visual models from natural language supervision," in *International conference on machine learning*. PmlR, 2021, pp. 8748–8763.
- [17] A. Dosovitskiy, "An image is worth 16x16 words: Transformers for image recognition at scale," *arXiv preprint arXiv:2010.11929*, 2020.
- [18] R. Zhang, Z. Guo, W. Zhang, K. Li, X. Miao, B. Cui, Y. Qiao, P. Gao, and H. Li, "Pointclip: Point cloud understanding by clip," in *Proceedings of the IEEE/CVF conference on computer vision and pattern recognition*, 2022, pp. 8552–8562.
- [19] J. Ji, H. Wang, C. Wu, Y. Ma, X. Sun, and R. Ji, "Jm3d & jm3d-llm: Elevating 3d representation with joint multi-modal cues," *IEEE Transactions on Pattern Analysis and Machine Intelligence*, vol. 47, no. 4, pp. 2475–2492, 2024.
- [20] R. Chen, Y. Liu, L. Kong, X. Zhu, Y. Ma, Y. Li, Y. Hou, Y. Qiao, and W. Wang, "Clip2scene: Towards label-efficient 3d scene understanding by clip," in *Proceedings of the IEEE/CVF Conference on Computer Vision and Pattern Recognition*, 2023, pp. 7020–7030.
- [21] S. Peng, K. Genova, C. Jiang, A. Tagliasacchi, M. Pollefeys, T. Funkhouser, *et al.*, "Openscene: 3d scene understanding with open vocabularies," in *Proceedings of the IEEE/CVF conference on computer vision and pattern recognition*, 2023, pp. 815–824.
- [22] G. Liao, J. Li, and X. Ye, "Vlm2scene: Self-supervised image-text-lidar learning with foundation models for autonomous driving scene understanding," in *Proceedings of the AAAI Conference on Artificial Intelligence*, vol. 38, no. 4, 2024, pp. 3351–3359.

- [23] S. Shubodh, M. Omama, H. Zaidi, U. S. Parihar, and M. Krishna, "Lip-loc: Lidar image pretraining for cross-modal localization," in *Proceedings of the IEEE/CVF Winter Conference on Applications of Computer Vision*, 2024, pp. 948–957.
- [24] Y. Wang, S. Huang, Y. Gao, Z. Wang, R. Wang, K. Sheng, B. Zhang, and S. Liu, "Transferring clip's knowledge into zero-shot point cloud semantic segmentation," in *Proceedings of the 31st ACM International Conference on Multimedia*, 2023, pp. 3745–3754.
- [25] Y. Lu, C. Xu, X. Wei, X. Xie, M. Tomizuka, K. Keutzer, and S. Zhang, "Open-vocabulary point-cloud object detection without 3d annotation," in *Proceedings of the IEEE/CVF conference on computer vision and pattern recognition*, 2023, pp. 1190–1199.
- [26] C. Pan, B. Yaman, S. Velipasalar, and L. Ren, "Clip-bevformer: Enhancing multi-view image-based bev detector with ground truth flow," in *Proceedings of the IEEE/CVF Conference on Computer Vision and Pattern Recognition*, 2024, pp. 15 216–15 225.
- [27] G. Hess, A. Tonderski, C. Petersson, K. Åström, and L. Svensson, "Lidarclip or: How i learned to talk to point clouds," in *Proceedings of the IEEE/CVF Winter Conference on Applications of Computer Vision*, 2024, pp. 7438–7447.
- [28] Y. Zeng, C. Jiang, J. Mao, J. Han, C. Ye, Q. Huang, D.-Y. Yeung, Z. Yang, X. Liang, and H. Xu, "Clip2: Contrastive language-image-point pretraining from real-world point cloud data," in *Proceedings of the IEEE/CVF conference on computer vision and pattern recognition*, 2023, pp. 15 244–15 253.
- [29] D. Hegde, J. M. J. Valanarasu, and V. Patel, "Clip goes 3d: Leveraging prompt tuning for language grounded 3d recognition," in *Proceedings of the IEEE/CVF International Conference on Computer Vision*, 2023, pp. 2028–2038.
- [30] L. Xue, M. Gao, C. Xing, R. Martín-Martín, J. Wu, C. Xiong, R. Xu, J. C. Niebles, and S. Savarese, "Ulip: Learning a unified representation of language, images, and point clouds for 3d understanding," in *Proceedings of the IEEE/CVF conference on computer vision and pattern recognition*, 2023, pp. 1179–1189.
- [31] X. Wang, G. Chen, G. Qian, P. Gao, X.-Y. Wei, Y. Wang, Y. Tian, and W. Gao, "Large-scale multi-modal pre-trained models: A comprehensive survey," *Machine Intelligence Research*, vol. 20, no. 4, pp. 447–482, 2023.
- [32] G. Cicchetti, E. Grassucci, and D. Comminiello, "A triangle enables multimodal alignment beyond cosine similarity," *arXiv preprint arXiv:2509.24734*, 2025.
- [33] H. Caesar, V. Bankiti, A. H. Lang, S. Vora, V. E. Liong, Q. Xu, A. Krishnan, Y. Pan, G. Baldan, and O. Beijbom, "nuscenes: A multimodal dataset for autonomous driving," *arXiv preprint arXiv:1903.11027*, 2019.
- [34] A. Geiger, P. Lenz, and R. Urtasun, "Are we ready for autonomous driving? the kitti vision benchmark suite," in *Conference on Computer Vision and Pattern Recognition (CVPR)*, 2012.
- [35] P. Sun, H. Kretzschmar, X. Dotiwalla, A. Chouard, V. Patnaik, P. Tsui, J. Guo, Y. Zhou, Y. Chai, B. Caine, V. Vasudevan, W. Han, J. Ngiam, H. Zhao, A. Timofeev, S. Ettinger, M. Krivokon, A. Gao, A. Joshi, Y. Zhang, J. Shlens, Z. Chen, and D. Anguelov, "Scalability in perception for autonomous driving: Waymo open dataset," in *Proceedings of the IEEE/CVF Conference on Computer Vision and Pattern Recognition (CVPR)*, June 2020.
- [36] J. Li, D. Li, C. Xiong, and S. Hoi, "Blip: Bootstrapping language-image pre-training for unified vision-language understanding and generation," in *International conference on machine learning*. PMLR, 2022, pp. 12 888–12 900.
- [37] L. Yao, R. Huang, L. Hou, G. Lu, M. Niu, H. Xu, X. Liang, Z. Li, X. Jiang, and C. Xu, "Filip: Fine-grained interactive language-image pre-training," *arXiv preprint arXiv:2111.07783*, 2021.
- [38] C. Jia, Y. Yang, Y. Xia, Y.-T. Chen, Z. Parekh, H. Pham, Q. Le, Y.-H. Sung, Z. Li, and T. Duerig, "Scaling up visual and vision-language representation learning with noisy text supervision," in *International conference on machine learning*. PMLR, 2021, pp. 4904–4916.
- [39] H. Xu, G. Ghosh, P.-Y. Huang, D. Okhonko, A. Aghajanyan, F. Metze, L. Zettlemoyer, and C. Feichtenhofer, "Videoclip: Contrastive pre-training for zero-shot video-text understanding," *arXiv preprint arXiv:2109.14084*, 2021.
- [40] A. Guzhov, F. Raue, J. Hees, and A. Dengel, "Audioclip: Extending clip to image, text and audio," in *ICASSP 2022-2022 IEEE International Conference on Acoustics, Speech and Signal Processing (ICASSP)*. IEEE, 2022, pp. 976–980.
- [41] X. Zhu, R. Zhang, B. He, Z. Guo, Z. Zeng, Z. Qin, S. Zhang, and P. Gao, "Pointclip v2: Prompting clip and gpt for powerful 3d open-world learning," in *Proceedings of the IEEE/CVF international conference on computer vision*, 2023, pp. 2639–2650.
- [42] R. Girdhar, A. El-Nouby, Z. Liu, M. Singh, K. V. Alwala, A. Joulin, and I. Misra, "Imagebind: One embedding space to bind them all," in *Proceedings of the IEEE/CVF conference on computer vision and pattern recognition*, 2023, pp. 15 180–15 190.
- [43] B. Zhu, B. Lin, M. Ning, Y. Yan, J. Cui, H. Wang, Y. Pang, W. Jiang, J. Zhang, Z. Li, *et al.*, "Languagebind: Extending video-language pretraining to n-modality by language-based semantic alignment," *arXiv preprint arXiv:2310.01852*, 2023.
- [44] T. Huang, B. Dong, Y. Yang, X. Huang, R. W. Lau, W. Ouyang, and W. Zuo, "Clip2point: Transfer clip to point cloud classification with image-depth pre-training," in *Proceedings of the IEEE/CVF International Conference on Computer Vision*, 2023, pp. 22 157–22 167.
- [45] F. Li, Z. Wang, Z. Huang, G. Dai, J. Wang, and M. Wang, "Triclip-3d: A unified parameter-efficient framework for tri-modal 3d visual grounding based on clip," *arXiv preprint arXiv:2507.14904*, 2025.
- [46] J. Zhou, J. Wang, B. Ma, Y.-S. Liu, T. Huang, and X. Wang, "Uni3d: Exploring unified 3d representation at scale," *arXiv preprint arXiv:2310.06773*, 2023.
- [47] M. Liu, R. Shi, K. Kuang, Y. Zhu, X. Li, S. Han, H. Cai, F. Porikli, and H. Su, "Openshape: Scaling up 3d shape representation towards open-world understanding," *Advances in neural information processing systems*, vol. 36, pp. 44 860–44 879, 2023.
- [48] L. Xue, N. Yu, S. Zhang, A. Panagopoulou, J. Li, R. Martín-Martín, J. Wu, C. Xiong, R. Xu, J. C. Niebles, *et al.*, "Ulip-2: Towards scalable multimodal pre-training for 3d understanding," in *Proceedings of the IEEE/CVF Conference on Computer Vision and Pattern Recognition*, 2024, pp. 27 091–27 101.
- [49] Q. Team, "Qwen3 technical report," 2025. [Online]. Available: <https://arxiv.org/abs/2505.09388>
- [50] J. Achiam, S. Adler, S. Agarwal, L. Ahmad, I. Akkaya, F. L. Aleman, D. Almeida, J. Altschmidt, S. Altman, S. Anadkat, *et al.*, "Gpt-4 technical report," *arXiv preprint arXiv:2303.08774*, 2023.
- [51] O. R. Musin and A. S. Tarasov, "The tammes problem for $n=14$," *Experimental Mathematics*, vol. 24, no. 4, pp. 460–468, 2015.
- [52] A. Vaswani, N. Shazeer, N. Parmar, J. Uszkoreit, L. Jones, A. N. Gomez, Ł. Kaiser, and I. Polosukhin, "Attention is all you need," *Advances in neural information processing systems*, vol. 30, 2017.
- [53] C. R. Qi, L. Yi, H. Su, and L. J. Guibas, "Pointnet++: Deep hierarchical feature learning on point sets in a metric space," *Advances in neural information processing systems*, vol. 30, 2017.
- [54] I. Loshchilov and F. Hutter, "Decoupled weight decay regularization," *arXiv preprint arXiv:1711.05101*, 2017.
- [55] M. Cherti, R. Beaumont, R. Wightman, M. Wortsman, G. Ilharco, C. Gordon, C. Schuhmann, L. Schmidt, and J. Jitsev, "Reproducible scaling laws for contrastive language-image learning," in *Proceedings of the IEEE/CVF conference on computer vision and pattern recognition*, 2023, pp. 2818–2829.